Assimilating Leaf Area Index Estimates from Remote Sensing into the Simulations of a Cropping Systems Model

K. R. Thorp, D. J. Hunsaker, A. N. French

Abstract. *Spatial extrapolation of cropping systems models for regional crop growth and water use assessment and farm-level precision management has been limited by the vast model input requirements and the model sensitivity to parameter uncertainty. Remote sensing has been proposed as a viable source of spatial information for guiding model simulations, but techniques for merging remote sensing with cropping systems models have not been rigorously explored. We developed and tested two techniques for assimilation of remotely sensed green leaf area index (GLAI) into the CSM-CROPSIM-CERES-Wheat model: one based on model "updating" and the other based on model "forcing". A dataset from two wheat irrigation scheduling experiments, conducted at Maricopa, Arizona, during the winters of 2003-2004 and 2004-2005, provided canopy spectral reflectance information and measurements of canopy weight, wheat yield, and evapotranspiration (ET) under varying planting densities and nitrogen rates for testing the ability of the assimilation techniques to improve model simulations. Monte Carlo simulation methods were used to assess the performance of GLAI data assimilation in light of uncertainty in the model parameters that govern the GLAI simulation. When considering this uncertainty, assimilation of GLAI by "updating" and by "forcing" was able to reduce error between measured and simulated canopy weight and ET by 43.6% and 56.5% and by 45.0% and 51.6%, respectively, as compared to the stand-alone model. The assimilation techniques had greater difficulty improving wheat yield simulations because simulated yield was more sensitive to parameters other than GLAI, especially in the 2004-2005 growing season. Assimilation of remotely sensed data into cropping systems models has potential to improve simulations of key model outputs, such as canopy weight and ET, but further efforts are warranted to explore and fine-tune techniques for merging these two technologies.*

Keywords. Biomass, CERES-Wheat, Crop model, Data assimilation, DSSAT, Evapotranspiration, Leaf area index, Monte Carlo, Remote sensing, Yield, Wheat.

Remote sensing and cropping systems modeling are two distinct technologies that have been developed to address diverse agronomic questions at field-level and regional scales (Whisler et al., 1986; Moran et al., 1997; Batchelor et al., 2002; Xie et al., 2008). Although these technologies have often been studied independently, there is growing interest in utilizing information derived from remote sensing to update or drive cropping systems model simulations because the two technologies are naturally complementary (Maas, 1988a; Moulin et al., 1998; Inoue, 2003; Dorigo et al., 2007). For example, whereas the daily time-step simulation capabilities of cropping systems models are excellent for crop growth analyses in the temporal domain, remote sensing images offer great opportunity to understand spatial crop growth patterns. Conversely, whereas model input requirements have limited the use of cropping systems models for spatial crop growth analyses, several

practical problems, including cloud cover and flight availability, have limited the reliability of remote sensing as a temporal crop analysis tool. With the integration of these technologies, the problems associated with one can be offset by the benefits of the other.

Several techniques for merging remote sensing data with model simulations, known collectively as "data assimilation" procedures, have been explored in past research. Simple approaches have utilized vegetation indices to update the value of key model state variables, such as green leaf area index (GLAI) or leaf weight, during the progression of seasonal simulations (Wiegand et al., 1986, Seidl et al., 2004; Hadria et al., 2006). Iterative techniques using optimization algorithms have also been used to "reinitialize" or "reparameterize" a model by adjusting initial conditions or input parameters to minimize error between simulated GLAI and remotely sensed estimates of GLAI (Maas, 1988b; Bouman, 1992; Clevers and van Leeuwen, 1996; Dente et al., 2008). In a similar way, linking a cropping systems model with a radiation transfer or canopy reflectance model allows recalibration procedures to be completed by directly comparing simulated and measured canopy reflectance (Moulin et al., 1995; Guérif and Duke, 1998; Weiss et al., 2001; Launay and Guerif, 2005). In most of the reported approaches for assimilating remote sensing data into cropping systems models, the authors have not accounted for measurement error in the remotely sensed estimates of model state variables (Seidl et al., 2004; Dente et al., 2008). More advanced data assimilation approaches, which implement ensemble Kalman filters to

The authors are **Kelly R. Thorp, ASABE Member Engineer,** Agricultural Engineer, **Douglas J. Hunsaker, ASABE Member Engineer,** Agricultural Engineer, and **Andrew N. French,** Physical Scientist; USDA-ARS U.S. Arid Land Agricultural Research Center, Maricopa, Arizona. **Corresponding author:** Kelly R. Thorp, USDA-ARS U.S. Arid Land Agricultural Research Center, 21881 N. Cardon Lane, Maricopa, AZ 85138; phone: 520-316-6375; fax: 520-316-6330; e-mail: kelly.thorp@ars.usda.gov.

combine simulated and observed state variables while accounting for the error in both, are also under development (Dorigo et al., 2007; Quaife et al., 2008).

The union of remote sensing and cropping systems modeling has been investigated for a diverse set of agricultural applications, including regional crop monitoring and yield prediction (Doraiswamy et al., 2004; Dente et al., 2008), precision crop management (Jones and Barnes, 2000; Seidl et al., 2004), and evapotranspiration mapping (Olioso et al., 2005). Because of the spatial nature of these applications, efforts to parameterize a cropping systems model for spatial simulations may be limited by a lack of information to describe the required cultivar, management, soil, and meteorological inputs for unique spatial units. This uncertainty in the model input parameters may degrade the predictive performance of the model, which data assimilation procedures aim to correct by periodically readjusting the simulation using spatial information from remote sensing images. Although this approach may sound reasonable for addressing the issue of limited model input data for spatial simulations, further evaluation efforts using thorough measured datasets are warranted to understand the feasibility of using remote sensing data to reliably update cropping systems model simulations.

The CSM-CROPSIM-CERES-Wheat model is one of the plant growth modules within the Cropping System Model (CSM ver. 4.5.0.036; Jones et al., 2003), as provided in the Decision Support System for Agrotechnology Transfer (DSSAT). Current and previous versions of this wheat (*Triticum aestivum* L.) growth model have been widely used to simulate the collective effect of cultivar characteristics, management practices, weather, and soil conditions on the growth, development, and yield of wheat plants, and the model has been shown to perform adequately for a wide selection of wheat varieties, climatic conditions, and soil types around the world (Chipanshi et al., 1999; Tubiello et al., 1999; Bannayan et al., 2003; Nain et al., 2004; Rinaldi, 2004; Lobell and Ortiz-Monasterio, 2006; Arora et al., 2007). Recently, Thorp et al. (2010) reported an evaluation of the CSM-CROPSIM-CERES-Wheat model using a thorough measured dataset from two wheat irrigation scheduling experiments conducted during the winters of 2003-2004 and 2004-2005 at Maricopa, Arizona. As a part of the data collection protocol for these experiments, treatment plots were intensively monitored using ground-based and aerial remote sensing in the thermal, visible, and near-infrared wavelengths. The measured dataset is ideal for testing approaches to assimilate remotely sensed information into CSM-CROPSIM-CERES-Wheat simulations. The objectives of this study were: (1) to develop strategies for assimilating remotely sensed estimates of GLAI into the CSM-CROPSIM-CERES-Wheat model, and (2) to demonstrate the ability of the data assimilation strategies to improve model simulations of canopy weight, wheat yield, and evapotranspiration (ET) in light of uncertainty in the model input parameters that govern GLAI.

MATERIALS AND METHODS

FIELD EXPERIMENTS

As reported by Hunsaker et al. (2007a, 2007b), ET estimation and irrigation scheduling experiments for wheat were conducted at the University of Arizona's Maricopa Agricul-

Table 1. Summary of subtreatments for the 2003-2004 and 2004-2005 FAO-56 irrigation scheduling experiments (FISE) for wheat.

| Subtreatment Abbreviation | Experimental Variables | | | No. of Replicates |
	K_{cb} Method	Plant Density	Nitrogen Level	
FSH	FAO (F)	Sparse (S)	High (H)	2
FSL	FAO (F)	Sparse (S)	Low (L)	2
FTH	FAO (F)	Typical (T)	High (H)	4
FTL	FAO (F)	Typical (T)	Low (L)	4
FDH	FAO (F)	Dense (D)	High (H)	2
FDL	FAO (F)	Dense (D)	Low (L)	2
NSH	NDVI (N)	Sparse (S)	High (H)	2
NSL	NDVI (N)	Sparse (S)	Low (L)	2
NTH	NDVI (N)	Typical (T)	High (H)	4
NTL	NDVI (N)	Typical (T)	Low (L)	4
NDH	NDVI (N)	Dense (D)	High (H)	2
NDL	NDVI (N)	Dense (D)	Low (L)	2

tural Center (MAC) near Maricopa, Arizona (33.067547° N, 111.97146° W) during the winters of 2003-2004 and 2004-2005. The soil type at the site was a Casa Grande sandy loam, classified as fine-loamy, mixed, hyperthermic, Typic Natrargids. The original objective for the research of Hunsaker et al. (2007a, 2007b) was to determine whether vegetation indices computed from canopy spectral reflectance measurements could be used to estimate basal crop coefficients (K_{cb}) required to compute crop ET and to schedule irrigations using FAO-56 methods (Allen et al., 1998). For both wheat experiments, the field layout consisted of 32 experimental plots, each 11.2×21 m and hydrologically isolated with border dikes. The main treatment consisted of two approaches for estimation of basal crop coefficients: one using a standard FAO-56 crop coefficient curve (F) as a function of days after emergence, and the other using a season-specific crop coefficient curve (N) based on remote sensing estimates of GLAI from normalized difference vegetation indices (NDVI). Subtreatments of plant density and nitrogen application rate were equally replicated within each main treatment to provide a range of crop growth and water use conditions (table 1). Three plant density levels, designated as sparse (S; ~75 plant m^{-2}), typical (T; ~150 plants m^{-2}), and dense (D; ~300 plants m^{-2}), were used. Nitrogen fertilizer was injected into irrigation pipes at two rates, giving seasonal nitrogen applications of ~80 kg N ha^{-1} for the low (L) treatment and ~215 kg N ha^{-1} for the high (H) treatment. A complete random design with incomplete blocks was used.

Hard red spring wheat (*Triticum aestivum* L., cv. Yecora Rojo) was planted at a 0.20 m row spacing on 10-12 December 2003 and on 22 December 2004. Irrigation border dikes were formed around each treatment plot, and raised board-walks on concrete blocks were installed for non-destructive access across the center of each plot. Two gated pipe irrigation lines were installed to flood irrigate individual treatment plots. Irrigation scheduling procedures based on the two scheduling approaches were initiated in early February for both seasons. Irrigations were scheduled for the day after soil water balance calculations demonstrated 45% depletion from total available root zone soil water. Applied irrigation amounts were 110% of depleted root zone soil water, where the extra 10% was to account for inefficiencies in the irrigation system. Nitrogen fertilizer was applied to each treatment plot by injecting 32% liquid urea ammonium nitrate into the gated pipe irrigation system.

FIELD MEASUREMENTS

Volumetric soil water contents were measured frequently at the center of each treatment plot. Neutron probes (model 503, Campbell Pacific Nuclear, Martinez, Cal.) were used to measure the soil moisture profile from 30 to 290 cm in 20 cm increments, and TDR probes (Trase1, Soil–Moisture Equipment Corp., Santa Barbara, Cal.) were used to measure soil moisture from the surface to a depth of 30 cm. Soil moisture measurements were collected at least weekly and always one day before and three to four days after an irrigation event. These soil moisture data were used to estimate the deep seepage and ET that occurred between soil moisture measurement dates based on the soil water balance method described by Hunsaker et al. (2005). Since model simulations were conducted to a depth of 210 cm in this study, neutron probe measurements from 210 cm to 290 cm were used to obtain an estimate of deep seepage. Actual ET was then computed by subtracting deep seepage from the total precipitation, irrigation, and change in soil water storage between soil moisture measurement dates.

Extensive agronomic measurements were collected to document wheat growth, development, and yield in each treatment plot. After wheat establishment, plant density measurements were collected to verify acceptability of the three plant density treatments. Phenology was documented weekly using the Zadoks et al. (1974) scale. Every two weeks following emergence, destructive plant sampling was used to measure various aspects of wheat growth, including canopy weight, leaf number, leaf weight, stem weight, spike weight, chaff weight, and grain weight. The green leaf area of dissected plant samples was measured using an area meter (model 3100, Li–Cor, Lincoln, Neb.), and green leaf area index was computed based on leaf area and plant density at emergence. On 26 May 2004 and 27 May 2005, a Hege plot combine (Wintersteiger AG, Ried im Innkreis, Austria) equipped with a 1.5 m cutter bar was used to collect grain samples from a 24 m^2 sample area delineated in the southern portion of each treatment plot.

Studies to characterize the physical properties of the soil at the field site were carried out in the spring of 2008, several years after the original field study. GPS navigation was used to collect soil samples at the original location of the 32 neutron access tubes. Laboratory analysis of these samples provided soil texture information for characterizing soil water retention and conductivity parameters. During both experiments, meteorological data was collected from an Arizona Meteorological Network (AZMET, http://cals.arizona.edu/azmet/) station located approximately 100 m north of the study area.

CANOPY REFLECTANCE MEASUREMENTS

Ground–based radiometric measurements were collected over each treatment plot two to four times per week from emergence to harvest using a four–band, hand–held radiometer (model BX–100, Exotech, Inc., Gaithersburg, Md.). The instrument was equipped with 15° field–of–view optics and positioned at a nadir view angle approximately 1.5 to 2.0 m above the soil surface. Data collection occurred in the morning around the time of a 57° solar zenith angle. Using board-walks for non–destructive plot access, 24 radiometric measurements of the crop canopy were collected along a 6 m east–west transect across the middle of each plot. Frequent radiometric observations of a calibrated, 0.6 m^2, 99% Spec-

tralon reflectance panel (Labsphere, Inc., North Sutton, N.H.) were used to characterize solar irradiance throughout the data collection period. Canopy reflectance factors in the red (610 to 680 nm) and near–infrared (NIR; 790 to 890 nm) were computed as the ratio of the average canopy radiance over the corresponding time–interpolated value for solar irradiance. The NDVI was computed from reflectance factors using the well–known equation:

$$NDVI = \left(\frac{NIR - Red}{NIR + Red} \right) \qquad (1)$$

Canopy reflectance measurements were available for computing NDVI on 29 and 31 dates during the 2003–2004 and 2004–2005 growing seasons, respectively.

The methods of Choudhury et al. (1994) were used to estimate wheat canopy cover and GLAI from the NDVI data collected during these experiments. Fractional vegetation cover (*f*) was computed from NDVI using:

$$f = 1 - \left(\frac{NDVI_{max} - NDVI}{NDVI_{max} - NDVI_{min}} \right)^{1/\xi} \qquad (2)$$

where NDVI measurements are rescaled according to the bare soil index (NDVI$_{min}$) and the full vegetation cover index (NDVI$_{max}$). The parameter ξ is a function of canopy leaf angle distribution with values near 1.4 for erectophile canopies and near 0.8 for planophile canopies. The GLAI was then computed from *f* according to:

$$GLAI = \left(\frac{\ln(1-f)}{-\beta} \right) \qquad (3)$$

where β is a second function of leaf angle distribution that ranges from 0.42 to 0.91. Based on the results of French et al. (2007), who used the measured GLAI and NDVI data from the 2004–2005 wheat experiment to parameterize these equations, we used values of 1.85 for ξ and 0.716 for β in all computations of GLAI from NDVI in the present study. For NDVI$_{min}$ and NDVI$_{max}$, we used 0.10 and 0.94, respectively.

CSM-CROPSIM-CERES-WHEAT

CSM–CROPSIM–CERES–Wheat is a computer program that utilizes carbon, nitrogen, and water balance principles to simulate the processes that occur during the growth and development of wheat plants within an agricultural system. The model calculates crop growth and development within a homogeneous area on a daily time step. Crop development proceeds through nine growth stages based on heat unit accumulation from planting to harvest. Carbon fixation is computed as a function incoming solar radiation, leaf area index, plant population, the canopy extinction coefficient, and radiation use efficiency. Fixed carbon is then partitioned to various plant parts, including leaves, stems, spikes, chaff, grain, and roots. Simulated plant growth responds to variation in management practices, crop cultivars, soil properties, and meteorological conditions. Management inputs required for model execution include plant population, row spacing, seed depth, planting and harvest dates, fertilizer application amounts and dates, and irrigation application amounts and dates. Cultivar parameters are used to define vernalization requirements, daylength sensitivity, radiation use efficiency, heat units needed to progress through growth stages, and

growth potentials for specific plant parts. Soils are defined by their water retention and conductivity characteristics, bulk density, pH, and initial conditions for water, inorganic nitrogen, and organic carbon. Daily inputs for minimum and maximum temperature, dew point temperature, solar radiation, wind run, and precipitation are also required. The model simulates plant stress effects from deficit and excess water conditions and from deficit nitrogen conditions, which feedback on the daily plant growth simulation.

A thorough evaluation of the CSM–CROPSIM–CERES–Wheat model for our wheat irrigation scheduling experiments was recently completed using all field measurements with exception of the canopy reflectance information (Thorp et al., 2010). Model calibration involved adjustment of cultivar parameters (table 2) to improve simulations of the average crop development, growth, and yield responses for the six standard FAO–56 treatments only. A single set of soil parameters (table 3) was specified to simulate the field–average soil moisture conditions for all standard FAO–56 treatments, which received identical irrigations. Based on the measurements of soil texture at the site, soil water retention and conductivity parameters were obtained from the Rosetta pedotransfer functions (Schaap et al., 2001). Data from the 2004–2005 experiment were used for model calibration, while data from the 2003–2004 experiment were used for independent model testing. The simulation controls, initial conditions, and input parameters resulting from the model evaluation (Thorp et al., 2010) were used as the baseline for simulations in the present study. As discussed below, further parameter adjustments using Monte Carlo methods were used to assess the performance of GLAI data assimilation techniques in light of uncertainty in several parameters that affect the calculation of GLAI.

DATA ASSIMILATION STRATEGIES

Assimilation of GLAI into the CSM–CROPSIM–CERES–Wheat model is expected to influence the crop growth simulation because the GLAI state variable is used to calculate the fraction of photosynthetically active radiation intercepted by the plant canopy (PARI). The equation used by the model to calculate daily PARI is:

$$PARI = 1.0 - e^{(-KCAN \cdot (GLAI + AWNAI))} \qquad (4)$$

where KCAN is the light extinction coefficient for photosynthetically active radiation, and AWNAI is the awn area index. The PARI state variable is then used in the daily rate equations to compute potential carbon fixation (PCARB, g plant^{-1}) according to:

$$PCARB = PARUV \cdot \left(\frac{PARAD}{PLTPOP} \right) \cdot PARI \qquad (5)$$

where PARUV (g MJ^{-1}) is the radiation use efficiency during vegetative development, PARAD (MJ m^{-2}) is the photosynthetically active radiation in the canopy (a function of the daily incoming solar radiation), and PLTPOP (plant m^{-2}) is the plant population. The radiation use efficiency can be specified uniquely during vegetative and reproductive development, so the input parameter for radiation use efficiency during reproductive development, PARUR (g MJ^{-1}), replaces PARUV in equation 5 during the reproductive phase (table 2). Actual carbon fixation for the plant system is then

Table 2. Calibrated cultivar parameters for the experimental dataset (Thorp et al., 2010).

Parameter	Description	Value
Crop Development		
PEG	Duration of phase from planting to germination ($^{\circ}$C d cm cm^{-1})[a]	75
PECM	Duration of phase from germination to emergence ($^{\circ}$C d cm^{-1})[a]	35
P1	Duration of phase from emergence to double ridges ($^{\circ}$C d)[b]	400
P1D	Percentage reduction in development rate in a photoperiod 10 h shorter than the threshold relative to that at the threshold[a]	12
P1V	Days at optimum vernalizing temperature required to complete vernalization[c]	5
P2	Duration of phase from double ridges to the end of leaf growth ($^{\circ}$C d)[a]	350
P3	Duration of phase from the end of leaf growth to the end of spike growth ($^{\circ}$C d)[a]	150
P4	Duration of phase from the end of spike growth to the end of the grain fill lag ($^{\circ}$C d)[a]	400
P5	Duration of the grain filling phase ($^{\circ}$C d)[a]	430
PHINT	Interval between successive leaf tip appearances ($^{\circ}$C d)[a]	105
TI1LF	Leaf number at which tillering begins[a]	1.5
Crop Growth		
PARUV	Conversion rate from photosynthetically active radiation to dry matter before the end of leaf growth (g MJ^{-1})[a]	2.2
PARUR	Conversion rate from photosynthetically active radiation to dry matter ratio after the end of leaf growth (g MJ^{-1})[a]	2.4
LAVS	Potential area of first-phase leaves (cm^2)[a]	25
LARS	Potential area of second-phase leaves (cm^2)[a]	50
LAWRS	Laminar area to weight ratio of first-phase leaves (cm^2 g^{-1})[b]	250
LAWR2	Laminar area to weight ratio of second-phase leaves (cm^2 g^{-1})[b]	230
Crop Yield		
G1	Kernel number per unit canopy weight at anthesis (kernels g^{-1})[a]	20
G2	Standard kernel size under optimum conditions (mg)[a]	54
G3	Standard, non-stressed dry weight of a single tiller at maturity (g)[b]	1.5
RSFRS	Fraction of fixed carbon partitioned to reserves prior to the end of stem growth[a]	0.12
GRNMN	Minimum grain nitrogen concentration (%)[a]	2.0
GRNS	Standard grain nitrogen concentration (%)[a]	3.0

[a] Parameter adjusted to improve measured versus simulated relationships.
[b] Parameter value selected from a subset of default values.
[c] Parameter value based on the results of Tubiello et al. (1999).

computed by reducing PCARB according to the current levels of temperature, water, and nitrogen stress. Based on equations 4 and 5, we expect the assimilation of remotely sensed estimates of GLAI to aid model simulations of total canopy weight. Crop yield simulations may also be improved, although many other parameters unrelated to the GLAI state variable are involved in the simulation of carbon partitioning and translocation of carbon to grain.

Table 3. Soil parameters obtained from the experimental dataset (Thorp et al., 2010).[a]

Depth (cm)	SLLL (cm cm^{-1})	SDUL (cm cm^{-1})	SSAT (cm cm^{-1})	SRGF (--)	SSKS (cm h^{-1})	SBDM (g cm^{-3})	SLOC (%)	SLCL (%)	SLSI (%)	SLHW (--)	SCEC (cmol kg^{-1})
0-5	0.093	0.226	0.407	1.000	1.5	1.49	0.58	21.0	10.8	8.3	12.0
5-15	0.093	0.226	0.407	1.000	1.5	1.49	0.58	21.0	10.8	8.3	12.0
15-30	0.093	0.226	0.407	1.000	1.5	1.49	0.58	21.0	10.8	8.3	12.0
30-45	0.099	0.228	0.435	0.657	2.0	1.40	0.17	22.6	10.8	8.3	12.0
45-60	0.103	0.249	0.431	0.432	1.9	1.42	0.17	24.1	10.7	8.3	12.0
60-90	0.106	0.251	0.399	0.186	1.2	1.53	0.17	24.0	12.5	8.3	12.0
90-120	0.098	0.247	0.382	0.080	1.0	1.58	0.17	21.4	11.8	8.3	12.0
120-150	0.078	0.234	0.377	0.035	1.7	1.58	0.17	16.9	9.2	8.3	12.0
150-180	0.088	0.221	0.380	0.015	1.3	1.58	0.17	19.2	9.4	8.3	12.0
180-210	0.088	0.251	0.380	0.006	1.3	1.58	0.17	19.2	9.4	8.3	12.0

[a] SLLL = lower limit, SDUL = drained upper limit, SSAT = saturated soil water content, SRGF = soil root growth factor,
SSKS = saturated hydraulic conductivity, SBDM = bulk density, SLOC = organic carbon content, SLCL = clay content,
SLSI = silt content, SLHW = pH in water, and SCEC = cation exchange capacity.

Assimilation of remotely sensed GLAI estimates into the CSM-CROPSIM-CERES-Wheat model is also expected to influence the water balance simulation because the GLAI state variable is used to calculate potential ET. Several methods are available for computing ET in the CSM, but we implemented the method based on modified FAO-56 procedures (Allen et al., 1998). With this method, the model uses the standard FAO-56 equations to compute daily reference ET (ET_o, mm d^{-1}) from the meteorological input data, and potential ET (PET, mm d^{-1}) is computed using a crop coefficient (K_c) approach:

$$PET = (K_c)ET_o \qquad (6)$$

The model then simulates actual ET to the extent that the simulated soil water supply can meet the PET demand and that the simulated plant system is able to extract and transpire that amount of water. The GLAI state variable influences PET, and thus actual ET, through its use in the calculation of K_c:

$$K_c = 1.0 + (EORATIO - 1.0) \cdot \left(\frac{GLAI}{6.0} \right) \qquad (7)$$

where EORATIO is a scaling parameter for adjusting the relationship between model-simulated GLAI and K_c. As reported by Thorp et al. (2010), the EORATIO parameter was calibrated to a value of 1.8 based on the experimental data.

Two strategies for assimilating GLAI data into CSM-CROPSIM-CERES-Wheat were considered in this work: one based on "updating" and the other based on "forcing" the GLAI state variable. The "updating" method adjusts the model only on the dates when GLAI observations are available. The "forcing" method adjusts the model on a daily time step using linear interpolation to compute GLAI between measurement dates. Assimilation of GLAI observations into the model simulation is more complex than simply overwriting the GLAI state variable because the daily growth rate equations are fundamentally focused at the individual plant level, while GLAI is an area-based variable. After computing daily growth for individual plants, the plant component weights are computed on an area basis using the plant population parameter, and GLAI is computed from the more fundamental plant leaf area (PLA, cm^2 plant^{-1}) state variable according to:

$$GLAI = (PLA - SENLA) \cdot PLTPOP \cdot 0.0001 \qquad (8)$$

where SENLA (cm^2 plant^{-1}) is the total leaf area that has been senesced from the plant, and PLTPOP (plants m^{-2}) is the plant population. To drive the model based on remotely sensed GLAI estimates, the model was reprogrammed to complete the following basic steps after it finished daily growth rate calculations:

- Read a file containing the remotely sensed GLAI observations.
- Compute (PLA-SENLA)$_{sim}$ as simulated by the model.
- Back-calculate (PLA-SENLA)$_{obs}$ by plugging the remotely sensed GLAI observation into equation 8.
- Compute the deficit plant leaf area: DEFICIT = (PLA-SENLA)$_{obs}$ - (PLA-SENLA)$_{sim}$.
- Adjust the PLA state variable by DEFICIT.

These steps effectively adjust the PLA state variable in the model such that GLAI is later computed (eq. 8) as the GLAI observed with remote sensing. Adjustment of the more fundamental PLA state variable ensures that the effects of the data assimilation are not lost during the growth rate calculations at the individual plant level on the following time step.

DATA ASSIMILATION EVALUATION

Although the model calibration described by Thorp et al. (2010) was based on extensive measured datasets obtained through field experimentation, simplifying assumptions in the model design and measurement error ultimately led to uncertainty in the model parameterization. Furthermore, remote sensing data assimilation will likely be most useful for applications in which a cropping systems model is extrapolated spatially at a field-level or regional scale, and detailed measured datasets will likely not be available for thorough calibration of a spatially extrapolated model. This would lead to even greater uncertainty in the model parameterization for the unique spatial units. Since the aim of remote sensing data assimilation is to correct for simulation errors that result from model parameter uncertainty, it is important to consider the effects of this uncertainty on the performance of the data assimilation strategies.

An analysis of model parameter uncertainty can be performed by first defining a probability distribution to describe the probable values for each model input parameter of interest. Parameter values are then iteratively and independently sampled from these distributions using Monte Carlo sampling techniques, which rely on a random number generator to computationally randomize the selection. Running the

cropping systems model for each sampled parameter set then demonstrates how the model outputs respond to the uncertainty in the model inputs (Monod et al., 2006).

To evaluate remotely sensed GLAI data assimilation while considering model parameter uncertainty in this work, Monte Carlo methods were used to randomly draw model parameter values from a normal distribution with mean equal to the calibrated value for several parameters. According to equation 8, GLAI is mainly affected by the plant population (PLTPOP) input parameter and the plant leaf area (PLA) state variable. The PLA state variable is mainly affected by the cultivar parameters that govern leaf growth (table 2), including the potential leaf areas (LAVS and LARS) and the laminar leaf area to leaf weight ratios (LAWRS and LAWR2). Monte Carlo methods were used to test the ability of GLAI data assimilation to improve model simulations while considering uncertainty in these model input parameters. Based on prior sensitivity analyses with the model, the standard deviations of the normal distributions from which the cultivar parameter values were drawn were specified as 3.0 cm^2 for LAVS and LARS and 20 cm^2 g^{-1} for LAWRS and LAWR2 (table 4). Standard deviations of the normal distributions from which PLTPOP parameters were drawn were based on variability in plant density measurements from emergence counts and biomass samples for each of the three planting densities in each season.

Using Monte Carlo methods, model simulations were performed for 10,000 unique sets of parameters. For each parameter set, simulations were completed for the six standard FAO-56 treatments (table 1) for both seasons of wheat irrigation scheduling experiments. For each of these twelve model runs, simulations were completed using GLAI data assimilation by the "updating" method, using GLAI data assimilation by the "forcing" method, and using no GLAI data assimilation. Simulation results for final canopy weight, wheat yield, and ET from emergence to physiological maturity were compiled. Simulated GLAI was also characterized by computing the GLAI integral (area under the curve) for each simulation.

Table 4. Definition of normal distributions from which parameter values were randomly drawn for Monte Carlo simulations.

Parameter	Description	Mean	SD[a]
LAVS	Potential area of first-phase leaves (cm^2)	25.0	3.0
LARS	Potential area of second-phase leaves (cm^2)	50.0	3.0
LAWRS	Laminar area to weight ratio of first-phase leaves (cm^2 g^{-1})	250.0	20.0
LAWR2	Laminar area to weight ratio of second-phase leaves (cm^2 g^{-1})	230.0	20.0
PLTPOP-S04	Sparse plant population for 2003-2004 season (plants m^{-2})	84.0	18.4
PLTPOP-T04	Typical plant population for 2003-2004 season (plants m^{-2})	164.0	33.0
PLTPOP-D04	Dense plant population for 2003-2004 season (plants m^{-2})	306.0	38.1
PLTPOP-S05	Sparse plant population for 2004-2005 season (plants m^{-2})	75.0	12.9
PLTPOP-T05	Typical plant population for 2004-2005 season (plants m^{-2})	155.0	32.7
PLTPOP-D05	Dense plant population for 2004-2005 season (plants m^{-2})	306.0	55.4

[a] SD = standard deviation.

A Python script (www.python.org) was written to automate the entire Monte Carlo simulation procedure.

RESULTS AND DISCUSSION
GLAI ESTIMATION FROM NDVI

As compared to measurements of GLAI from biomass samples for the standard FAO-56 treatments at the site, GLAI was estimated from NDVI with RMSEs of 0.47 and 0.41 for the 2003-2004 and 2004-2005 wheat growing seasons, respectively (fig. 1). This result demonstrates a relationship between the measured and NDVI-estimated GLAI values, although it is important to note the limitations of each of these methods for determining GLAI. Direct measurement of GLAI is labor-intensive, slow, and intrusive, and appropriate plant sampling techniques are required for precise measurements (Tewolde et al., 2005). Our GLAI measurements were based on the leaf area of six median-sized plants sampled from two 0.5 m row lengths. Clearly, the ability of these six plants to represent the GLAI status of the entire treatment plot on a particular measurement date may be questionable. The GLAI computation from the leaf area of the six plants was also highly sensitive to the plant density, which could vary depending on which biomass sample was used to determine the plant density. Ultimately, the plant counts collected at emergence were used to estimate the plant density of each plot for computation of GLAI on all biomass sampling dates. These limitations of the direct GLAI measurement approach were circumvented by estimating GLAI from NDVI measurements. Since reflectance scans were collected over a relatively large area of crop canopy each time, the NDVI-estimated GLAI are potentially more representative of the actual plot-level GLAI status. On the other hand, crop canopy reflectance data are known to be sensitive to a variety of factors, including solar zenith angle, atmospheric conditions, soil background effects, instrument limitations, and data calibration techniques. Additional error can certainly result from the assumptions of the empirical relationships used to produce GLAI from the NDVI measurements (eqs. 2 and 3).

For many of the treatments, the seasonal GLAI time-series as estimated from the NDVI measurements (fig. 2b) was typically smoother than the GLAI time-series based on biomass measurements (fig. 2a). This characteristic tended to facilitate the assimilation of the NDVI-estimated GLAI into the cropping systems model, without extreme disruption of the simulation progression due to unrealistic jumps in the assimilated GLAI values. In comparing the "updating" and "forcing" data assimilation methods, the resulting difference in simulated GLAI was often quite small when assimilating the NDVI-estimated GLAI (fig. 2b). Assimilating the measured GLAI values often resulted in a substantial difference between the simulated GLAI under the "updating" and "forcing" methodologies as well as several unrealistic discontinuities in simulated GLAI (fig. 2a). Figure 2 demonstrates these results using simulations from the fully calibrated FAO-56, dense population, low nitrogen (FDL) treatment for data collected during the 2003-2004 growing season. As shown in figure 2, assimilation of both GLAI datasets resulted in a GLAI simulation that deviated from the model-only simulations of GLAI. We conclude that reliable estimates of GLAI can be derived from spectral reflectance measurements of the
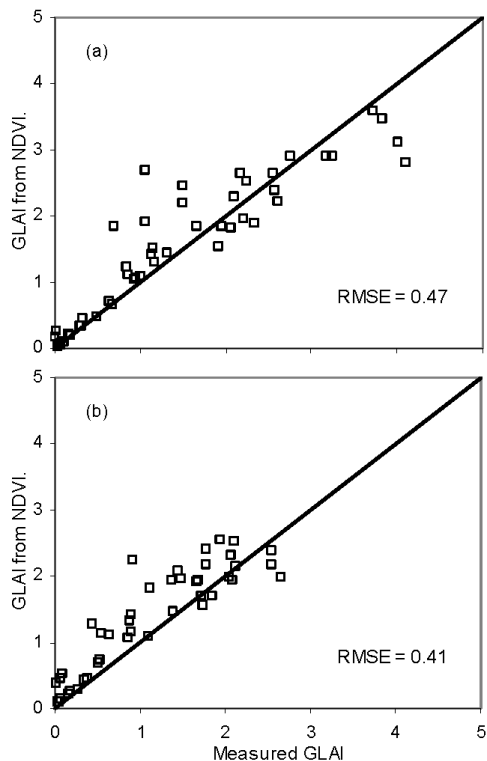
Figure 1. Relationship between average measured green leaf area index (GLAI) and average GLAI estimated from normalized difference vegetation indices (NDVI) for the six standard FAO–56 treatments during the (a) 2003–2004 and (b) 2004–2005 wheat experiments.
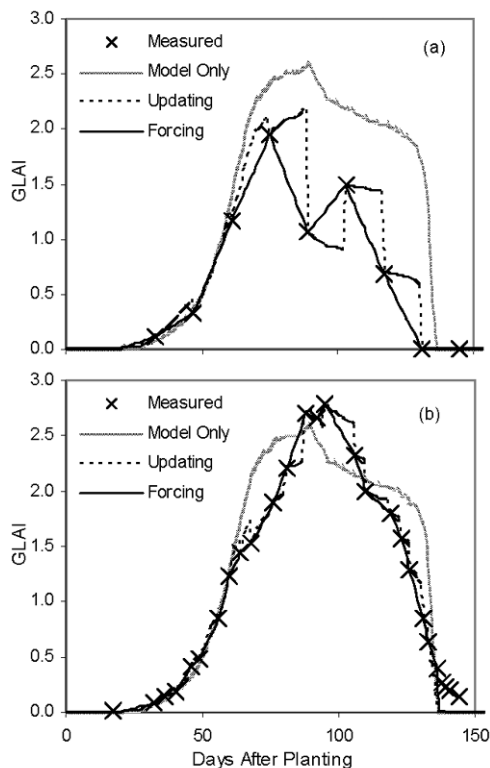

Figure 2. Example of simulated green leaf area index (GLAI) using "updating" and "forcing" data assimilation methodologies when GLAI was (a) measured from biomass samples and (b) estimated from normalized difference vegetation indices (NDVI) of the crop canopy. Model–only simulated GLAI is shown for comparison.
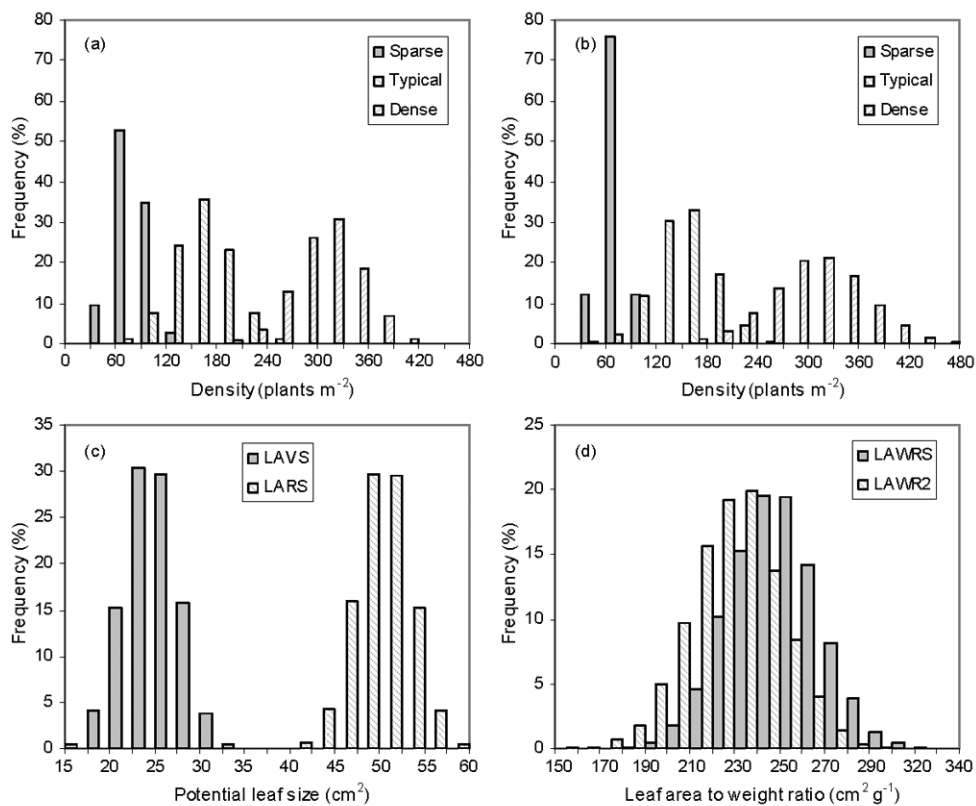
Figure 3. Histograms of sampled parameter values using Monte Carlo methods for plant density in the (a) 2003–2004 and (b) 2004–2005 growing seasons and for (c) two parameters that define potential leaf size and (d) two parameters that define leaf area to weight ratios.

crop canopy, and we can use those estimates to make reasonable adjustments to the GLAI state variable of the wheat growth model over the course of its simulation timeframe.

MONTE CARLO SIMULATIONS

For Monte Carlo simulations to be useful, model parameters needed to be sampled from their respective normal distributions enough times to adequately represent the domain of possible outcomes. Our selection of 10,000 iterations was rather arbitrary and was based mainly on the amount of time required to run the model, but results demonstrated that the selected parameter values adequately represented the sampling space and were normally distributed (fig. 3). For all the parameters, the percent differences between the requested means (table 4) and the actual Monte Carlo sample means were not greater than 0.3%. Likewise, the percent difference between the requested standard deviations (table 4) and the

actual Monte Carlo sample standard deviations were not greater than 1.6%. We conclude that 10,000 iterations of the Monte Carlo procedure were adequate for selecting parameter sets that reasonably estimated the possible uncertainty in the aspects of the model parameterization that most greatly influence the GLAI simulation.

GLAI DATA ASSIMILATION

Monte Carlo simulations demonstrated two important aspects of the data assimilation approaches, including reductions in the variability of the model output as compared to model–only simulations and improvements in the average simulated model output as compared to measurements (fig. 4). When the GLAI data assimilation approaches accomplished one or both of these, we conclude that they offer some value over using the model alone when considering the potential for uncertainty in the model parameterization.
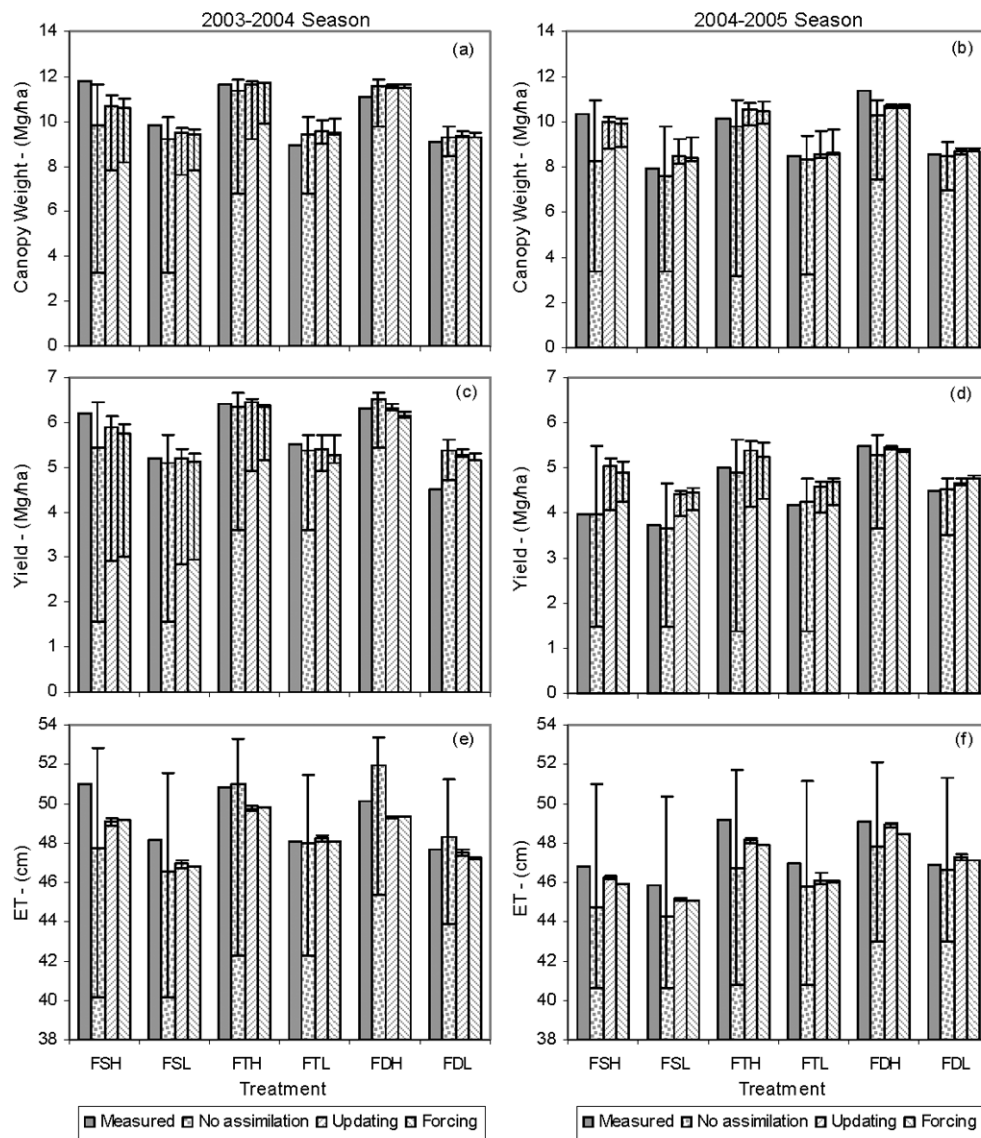

Figure 4. Average simulated final canopy weight (a and b), wheat yield (c and d), and evapotranspiration (e and f) when using no GLAI data assimilation, GLAI data assimilation by "updating", and GLAI data assimilation by "forcing" for the six experimental treatments during the 2003–2004 (left) and 2004–2005 (right) growing seasons. Treatments included FAO–56 (F) crop coefficient approaches for sparse (S), typical (T), and dense (D) plant populations and high (H) and low (L) nitrogen rates. Error bars show the maximum and minimum simulation results when using Monte Carlo methods to consider uncertainty in the model input parameters that affect GLAI. Measured values from field experiments are also provided.

Simulations with the stand-alone model demonstrated the model's sensitivity to uncertainty in the five input parameters that were adjusted for each simulation, i.e., plant population (PLTPOP), potential area of first-phase leaves (LAVS), potential area of second-phase leaves (LARS), laminar area to weight ratio of first-phase leaves (LAWRS), and laminar area to weight ratio of second-phase leaves (LAWR2). When GLAI data assimilation was not used, simulations of final canopy weight varied widely within individual treatments, with much greater variation for sparse plant density treatments than for dense plant density treatments. For example, final canopy weight for simulations without data assimilation ranged from 3.3 to 11.7 Mg ha^{-1} for the FSH treatment in the 2003-2004 growing season, while the range for the FDL treatment was 8.4 to 9.8 Mg ha^{-1} (fig. 4a). However, when GLAI data assimilation based on remote sensing was implemented, the range of variability in final canopy weight was substantially reduced for all treatments in both growing seasons (figs. 4a and 4b). For example, by "updating" the GLAI state variable, final canopy weight was simulated from 7.9 to 11.1 Mg ha^{-1} for the FSH treatment and from 9.3 to 9.5 Mg ha^{-1} for the FDL treatment in the 2003-2004 growing season (fig. 4a). By "forcing" the GLAI state variable, final canopy weight in the same growing season was simulated from 8.2 to 11.0 Mg ha^{-1} for the FSH treatment and from 9.3 to 9.5 Mg ha^{-1} for the FDL treatment. These results demonstrate little difference in the effects of "updating" versus "forcing" assimilation approaches on final canopy weight simulations, which was expected since GLAI inputs for each method were not largely different (fig. 2b).

Similar conclusions with regard to the variability in model output can be drawn for yield (figs 4c and 4d) and for ET simulations (figs. 4e and 4f). Typically, the variability in yield and ET outputs tended to decrease from sparse to typical to dense plant density treatments, and there was often relatively little difference between the yield and ET simulations when comparing the "updating" and "forcing" data assimilation approaches. But most importantly, when using Monte Carlo methods to consider uncertainty in the parameters that define plant density and leaf growth characteristics, simulations without GLAI data assimilation always resulted in greater variability in yield and ET as compared to simulations that incorporated GLAI data assimilation based on remote sensing. Thus, for applications in which uncertainty in these parameters may be considerable, particularly those that spatially extrapolate this one-dimensional model, estimates of GLAI from remote sensing images may reduce the sensitivity of the model to these input parameters and may narrow the possible range of outputs for canopy weight, yield, and ET.

In addition to reducing variability in the model outputs, data assimilation approaches also often improved the average simulated model output in relation to measured values at the field site. As an example for the FSH treatment in the 2003-2004 growing season, the errors between average measured and simulated canopy weights were 1.9, 1.1, and 1.1 Mg ha^{-1} for model-only simulations, "updating" assimilation, and "forcing" assimilation, respectively (fig. 4a). For FSH in the 2004-2005 growing season, these errors between average measured and simulated canopy weights were 2.0, 0.3, and 0.4 Mg ha^{-1}, respectively. The magnitude of the improvement in the canopy weight simulations was lower for other treatments, but generally the results demonstrated fa-

vorable adjustments of the simulations to reduce error between average measured and simulated canopy weights when using the GLAI data assimilation approaches. For 2003-2004, FTL was the only treatment in which data assimilation approaches worsened canopy weight simulations (fig. 4a), although only very slightly. For 2004-2005, FSL was the only treatment in which data assimilation approaches worsened canopy weight simulations (fig. 4b), although the GLAI assimilation did bump the canopy weight in the appropriate direction with respect to the error between measured and model-only values.

Data assimilation also improved average wheat yield simulations as compared to measured values for most of the treatments in the 2003-2004 growing seasons. In particular, for the FSH treatment, the errors between average measured and simulated yield were 0.8, 0.3, and 0.4 Mg ha^{-1} for model-only simulations, "updating" assimilation, and "forcing" assimilation, respectively (fig. 4c). The only exception was the "forcing" assimilation procedure for the FTL treatment, which increased the error between measured and simulated yield to 0.3 Mg ha^{-1}, as compared to 0.2 Mg ha^{-1} for the model-only simulations. Notice that for the FSH and FSL treatments, the stand-alone model tended to underestimate yield and the GLAI assimilation techniques bumped the average yield simulations upward, while for the FDH and FDL treatments, the stand-alone model tended to overestimate yield and the GLAI assimilation techniques bumped the average yield simulation downward. This result highlights how the GLAI assimilation can adjust the simulation appropriately based assessments of local crop growth conditions using remote sensing. Although data assimilation generally demonstrated positive effects on average wheat yield simulations for the 2003-2004 growing season, results were less favorable for the 2004-2005 growing season (fig. 4d). In the second year, GLAI data assimilation resulted in improvements in average wheat yield only for the FDH treatment. In all other treatments, the average wheat yield for model-only simulations more closely agreed with measurements, and both assimilation approaches resulted in an overestimation of yield. This is likely related to the fact that GLAI mainly influences total canopy weight, through equations 4 and 5, but many other parameters are involved in the simulation of kernel set, kernel size, partitioning of fixed carbon to grain, and ultimately wheat yield. Because later fertigations caused higher nitrogen stress levels in 2004-2005 (Hunsaker et al., 2007a), yield simulations in this season were highly sensitive to two parameters that govern nitrogen concentration in grain and its effect on crop yield (Thorp et al., 2010). This aspect of the simulation was likely the driver of 2004-2005 simulated yield and likely contributed to the poor performance of the GLAI assimilation for yield in this season. In spite of this, data assimilation substantially reduces the variability of 2004-2005 simulated wheat yields in response to uncertainty in the parameters that drive the GLAI simulation.

Error between average measured and simulated ET was reduced for many of the treatments in 2003-2004. As an example, for the FSH treatment in 2003-2004, the errors between average measured and simulated ET were 3.3, 1.9, and 1.9 cm for model-only simulations, "updating" assimilation, and "forcing" assimilation, respectively (fig. 4e). Only the FTH treatment in 2003-2004 had higher error between average measured and simulated ET, which resulted mainly from an overcompensation of the assimilation approaches to re-

duce the simulated ET. In 2004-2005, the stand-alone model tended to underestimate ET for all six treatments, and both GLAI data assimilation approaches reduced error between average measured and simulated ET for all six treatments (fig. 4f). The data assimilation procedures also resulted in notable reductions in the variability of the ET simulation in response to uncertainty in the parameters that drive GLAI. In fact, the variability in ET simulations for the "forcing" method is quite negligible for all the treatments in both seasons (figs. 4e and 4f), indicating that this method has nearly eliminated the influence of the plant density and leaf growth input parameters on the simulation of ET. These results demonstrate very favorable responses of the ET simulation to the data assimilation approaches.

The ability of GLAI data assimilation to reduce error between measured and simulated values for canopy weight, yield, and ET as compared to model-only simulations was related to two conditions (table 5). The first condition was whether the GLAI data assimilation procedure increased or decreased the GLAI integral (area under the GLAI curve) in relation to that of the stand-alone model. The second condition was whether the stand-alone model underestimated or overestimated canopy weight, yield, or ET in relation to measurements. For example, simulations of final canopy weight were brought closer to measurements in 83.1% of the cases in which the stand-alone model underestimated final canopy weight and data assimilation by "updating" increased the GLAI integral. Given that higher GLAI leads to greater carbon fixation (eqs. 4 and 5), we expected a high percentage of simulations to be improved under these conditions. However, when the stand-alone model already overestimated canopy weight and "updating" assimilation further increased the GLAI integral, canopy weight was improved in only 13.4% of cases. When the "updating" assimilation decreased the GLAI integral in relation to that of the stand-alone model, error between measured and simulated canopy weight was reduced for 65.3% of cases in which the stand-alone model overestimated canopy weight but for 53.0% of cases in which the stand-alone model had already underestimated the canopy weight. As expected, simulations of canopy weight were improved for a higher percentage of cases in which the stand-alone model had overestimated the canopy weight and data assimilation reduced the GLAI integral. This is likely the result of reduced carbon fixation (eqs. 4 and 5) with lower simulated GLAI. As demonstrated in table 5, similar conditions increased the chances of improving simulations of wheat yield and ET using the "updating" and "forcing" GLAI assimilation approaches. In particular for ET, GLAI data assimilation was more likely to reduce error between measured and simulated ET when the stand-alone model underestimated ET and assimilation procedures increased the GLAI integral, since higher GLAI increased the simulated potential evapotranspiration (eqs. 6 and 7). Likewise, if the stand-alone model overestimated ET, then improvements in the ET simulation were obtained more often when data assimilation reduced the GLAI integral.

In summary, when the stand-alone model underestimated final canopy weight, yield, or ET, the data assimilation approaches were more effective when the assimilated GLAI from remote sensing increased the simulated GLAI as compared to the stand-alone model. Conversely, when the stand-alone model overestimated final canopy weight, yield,

Table 5. Percent of cases in which GLAI data assimilation reduced error between measured and simulated final canopy weight, wheat yield, and evapotranspiration (ET) as compared to the stand-alone model for conditions of underestimation (UE) or overestimation (OE) by the stand-alone model and conditions of increasing (INC) or decreasing (DEC) the GLAI integral.

GLAI Integral	Stand-Alone Model					
	Canopy Weight		Wheat Yield		ET	
	UE	OE	UE	OE	UE	OE
"Updating" effect on GLAI						
INC	**83.1**	13.4	**62.7**	4.6	**87.7**	46.8
DEC	53.0	**65.3**	44.9	**79.4**	10.0	**78.1**
"Forcing" effect on GLAI						
INC	**85.5**	18.3	**53.4**	9.2	**85.6**	51.7
DEC	42.2	**74.6**	14.7	**60.2**	3.6	**75.6**

or ET, the data assimilation approaches were more effective when the assimilated GLAI from remote sensing decreased the simulated GLAI as compared to the stand-alone model. Lending further support to the performance of the GLAI data assimilation approaches is the fact that one of these two conditions was true for 77%, 72%, and 91% of the of the total simulations for canopy weight, wheat yield, and ET, respectively. Thus, the data assimilation approaches tended to reduced error between measured and simulated canopy weight, yield, and ET as compared to the stand-alone model for a majority of the total simulations. Overall, data assimilation by "updating" improved simulations of canopy weight, wheat yield, and ET for 66.6%, 53.7%, and 79.4% of the total simulations (10,000 Monte Carlo runs for each of the six experimental treatments in two growing seasons), respectively. Likewise, data assimilation by "forcing" improved simulations of canopy weight, wheat yield, and ET for 69.6%, 43.3%, and 77.2% of the total simulations, respectively. Over all the simulations, data assimilation by "updating" reduced error between measured and simulated canopy weight, wheat yield, and ET by 43.6%, 0.6%, and 56.5%, respectively, as compared to the stand-alone model. Likewise, data assimilation by "forcing" reduced error between measured and simulated canopy weight, yield, and ET by 45.0%, -9.8%, and 51.6%, respectively, as compare to model-only simulations.

CONCLUSIONS

- Estimates of green leaf area index (GLAI), obtained from spectral reflectance measurements of wheat canopies, can be used to alter the progression of CSM-CROPSIM-CERES-Wheat simulations by overwriting the plant leaf area (PLA) state variable such that the model computes GLAI as estimated from remote sensing.
- Monte Carlo methods were effective for testing the performance of GLAI data assimilation in light of uncertainty in the model parameters that govern the GLAI simulation.
- Assimilation of remotely sensed GLAI into the CSM-CROPSIM-CERES-Wheat model improved simulations of final canopy weight, wheat yield, and evapotranspiration (ET) by improving the average simulated model output in relation to measurements and by reducing the variability of the model output as compared to model-only simulations.

- Assimilation of remotely sensed GLAI into the CSM-CROPSIM-CERES-Wheat model was more likely to improve simulations of final canopy weight, wheat yield, and ET when GLAI and the output variable were both either underestimated or overestimated by the stand-alone model.
- There was no apparent trend in the ability of the "updating" assimilation technique to outperform the "forcing" assimilation technique, and vice versa.

REFERENCES

Allen, R. G., L. S. Pereira, D. Raes, and M. Smith. 1998. Crop evapotranspiration: Guidelines for computing crop water requirements. FAO Irrigation and Drainage Paper 56. Rome, Italy: Food and Agriculture Organization of the United Nations.

Arora, V. K., H. Singh, and B. Singh. 2007. Analyzing wheat productivity responses to climatic, irrigation, and fertilizer-nitrogen regimes in semi-arid sub-tropical environment using the CERES-Wheat model. *Agric. Water Mgmt.* 94(1-3): 22-30.

Bannayan, M., N. M. J. Crout, and G. Hoogenboom. 2003. Application of the CERES-Wheat model for within-season prediction of winter wheat yield in the United Kingdom. *Agron. J.* 95(1): 114-125.

Batchelor, W. D., B. Basso, and J. O. Paz. 2002. Examples of strategies to analyze spatial and temporal yield variability using crop models. *European J. Agron.* 18(2): 141-158.

Bouman, B. A. M. 1992. Linking physical remote sensing models with crop growth simulation models, applied for sugar beet. *Intl. J. Remote Sensing* 13(14): 2565-2581.

Chipanshi, A. C., E. A. Ripley, and R. G. Lawford. 1999. Large-scale simulation of wheat yields in a semi-arid environment using a crop-growth model. *Agric. Systems* 59(1): 57-66.

Choudhury, B. J., N. U. Ahmed, S. B. Idso, R. J. Reginato, and C. S. T. Daughtry. 1994. Relations between evaporation coefficients and vegetation indices studies by model simulations. *Remote Sensing Environ.* 50(1): 1-17.

Clevers, J. G. P. W., and H. J. C. van Leeuwen. 1996. Combined use of optical and microwave remote sensing data for crop growth monitoring. *Remote Sensing Environ.* 56(1): 42-51.

Dente, L., G. Satalino, F. Mattia, and M. Rinaldi. 2008. Assimilation of leaf area index derived from ASAR and MERIS data into CERES-Wheat model to map wheat yield. *Remote Sensing Environ.* 112(4): 1395-1407.

Doraiswamy, P. C., J. L. Hatfield, T. J. Jackson, B. Akhmedov, J. Prueger, and A. Stern. 2004. Crop condition and yield simulations using LANDSAT and MODIS. *Remote Sensing Environ.* 94(4): 548-559.

Dorigo, W. A., R. Zurita-Milla, A. J. W. de Wit, J. Brazile, R. Singh, and M. E. Schaepman. 2007. A review on reflective remote sensing and data assimilation techniques for enhanced agroecosystem modeling. *Intl. J. Applied Earth Observation and Geoinformation* 9(2): 165-193.

French, A. N., D. J. Hunsaker, T. R. Clarke, G. J. Fitzgerald, W. E. Luckett, and P. J. Pinter Jr. 2007. Energy balance estimation of evapotranspiration for wheat grown under variable management practices in central Arizona. *Trans. ASABE* 50(6): 2059-2071.

Guérif, M., and C. Duke. 1998. Calibration of the SUCROS emergence and early growth module for sugar beet using optical remote sensing data assimilation. *European J. Agron.* 9(2-3): 127-136.

Hadria R., B. Duchemin, A. Lahrouni, S. Khabba, S. Er-Raki, G. Dedieu, A. G. Chehbouni, and A. Olioso. 2006. Monitoring of irrigated wheat in a semi-arid climate using crop modelling and remote sensing data: Impact of satellite revisit time frequency. *Intl. J. Remote Sensing* 27(6): 1093-1117.

Hunsaker, D. J., E. M. Barnes, T. R. Clarke, G. J. Fitzgerald, and P. J. Pinter Jr. 2005. Cotton irrigation scheduling using remotely sensed and FAO-56 basal crop coefficients. *Trans. ASAE* 48(4): 1395-1407.

Hunsaker, D. J., G. J. Fitzgerald, A. N. French, T. R. Clarke, M. J. Ottman, and P. J. Pinter Jr. 2007a. Wheat irrigation management using multispectral crop coefficients: I. Crop evapotranspiration prediction. *Trans. ASABE* 50(6): 2017-2033.

Hunsaker, D. J., G. J. Fitzgerald, A. N. French, T. R. Clarke, M. J. Ottman, and P. J. Pinter Jr. 2007b. Wheat irrigation management using multispectral crop coefficients: II. Irrigation scheduling performance, grain yield, and water use efficiency. *Trans. ASABE* 50(6): 2035-2050.

Inoue, Y. 2003. Synergy of remote sensing and modeling for estimating ecophysiological processes in plant production. *Plant Production Sci.* 6(1): 3-16.

Jones, D., and E. M. Barnes. 2000. Fuzzy composite programming to combine remote sensing and crop models for decision support in precision crop management. *Agric. Systems* 65(3): 137-158.

Jones, J. W., G. Hoogenboom, C. H. Porter, K. J. Boote, W. D. Batchelor, L. A. Hunt, P. W. Wilkens, U. Singh, A. J. Gijsman, and J. T. Ritchie. 2003. The DSSAT cropping systems model. *European J. Agron.* 18(3-4): 235-265.

Launay, M., and M. Guerif. 2005. Assimilating remote sensing data into a crop model to improve predictive performance for spatial applications. *Agric., Ecosystems, and Environ.* 111(1-4): 321-339.

Lobell, D. B., and J. I. Ortiz-Monasterio. 2006. Evaluating strategies for improved water use in spring wheat with CERES. *Agric. Water Mgmt.* 84(3): 249-258.

Maas, S. J. 1988a. Use of remotely-sensed information in agricultural crop growth models. *Ecological Modelling* 41(3-4): 247-268.

Maas, S. J. 1988b. Using satellite data to improve model estimates of crop yield. *Agron. J.* 80(4): 655-662.

Monod, H., C. Naud, and D. Makowski. 2006. Uncertainty and sensitivity analysis for crop models. In *Working with Dynamic Crop Models: Evaluation, Analysis, Parameterization, and Applications*, 55-96. D. Wallach, D. Makowski, and J. W. Jones, eds. Amsterdam, The Netherlands: Elsevier.

Moulin, S., A. Fischer, G. Dedieu, and R. Delecolle. 1995. Temporal variations in satellite reflectances at field and regional scales compared with values simulated by linking crop growth and SAIL models. *Remote Sensing Environ.* 54(3): 261-272.

Moulin, S., A. Bondeau, and R. Delecolle. 1998. Combining agricultural crop models and satellite observations: From field to regional scales. *Intl. J. Remote Sensing* 19(6): 1021-1036.

Moran, M. S., Y. Inoue, and E. M. Barnes. 1997. Opportunities and limitations for image-based remote sensing in precision crop management. *Remote Sensing of Environ.* 61(3): 319-346.

Nain, A. S., V. K. Dadwal, and T. P. Singh. 2004. Use of CERES-Wheat model for wheat yield forecast in central Indo-Gangetic Plains of India. *J. Agric. Sci.* 142(1): 59-70.

Olioso, A., Y. Inoue, S. Ortega-Farias, J. Demarty, J.-P. Wigneron, I. Braud, F. Jacob, P. Lecharpentier, C. Ottlé, J.-C. Calvet, and N. Brisson. 2005. Future directions for advanced

evapotranspiration modeling: Assimilation of remote sensing data into crop simulation models and SVAT models. *Irrig. and Drainage Systems* 19(3-4): 377-412.

Quaife T., P. Lewis, M. De Kauwe, M. Williams, B. E. Law, M. Disney, and P. Bowyer. 2008. Assimilating canopy reflectance data into an ecosystem model with an ensemble Kalman filter. *Remote Sensing Environ*. 112(4): 1347-1364.

Rinaldi, M. 2004. Water availability at sowing and nitrogen management of durum wheat: A seasonal analysis with the CERES-Wheat model. *Field Crops Res*. 89(1): 27-37.

Schaap, M. G., F. J. Leij, and M. T. Van Genuchten. 2001. ROSETTA: A computer program for estimating soil hydraulic parameters with hierarchical pedotransfer functions. *J. Hydrol.* 251(3-4): 163-176.

Seidl, M. S., W. D. Batchelor, and J. O. Paz. 2004. Integrating remotely sensed images with a soybean model to improve spatial yield simulation. *Trans. ASAE* 47(6): 2081-2090.

Tewolde, H., K. R. Sistani, D. E. Rowe, A. Adeli, and T. Tsegaye. 2005. Estimating cotton leaf area index nondestructively with a light sensor. *Agron. J*. 97(4): 1158-1163.

Thorp, K. R., D. J. Hunsaker, A. N. French, J. W. White, T. R. Clarke, and P. J. Pinter Jr. 2010. Evaluation of the CSM-CROPSIM-CERES-Wheat model as a tool for crop water management. *Trans. ASABE* 53(1): 87-102.

Tubiello, F. N., C. Rosenzweig, B. A. Kimball, P. J. Pinter Jr., G. W. Wall, D. J. Hunsaker, R. L. LaMorte, and R. L. Garcia. 1999. Testing CERES-Wheat with Free-Air Carbon Dioxide Enrichment (FACE) experiment data: CO_2 and water interactions. *Agron. J*. 91(2): 247-255.

Weiss M., D. Troufleau, F. Baret, H. Chauki, L. Prévot, A. Olioso, N. Bruguier, and N. Brisson. 2001. Coupling canopy functioning and radiative transfer models for remote sensing data assimilation. *Agric. and Forest Meteorology* 108(2): 113-128.

Whisler, F. D., B. Acock, D. N. Baker, R. E. Fye, H. F. Hodges, J. R. Lambert, H. E. Lemmon, J. M. McKinion, and V. R. Reddy. 1986. Crop simulation models in agronomic systems. *Advances in Agron*. 40: 141-208.

Wiegand, C. L., A. J. Richardson, R. D. Jackson, P. J. Pinter Jr., J. K. Aase, D. E. Smika, L. F. Lautenschlager, and J. E. McMurtrey III. 1986. Development of agrometeorological crop model inputs from remotely sensed information. *IEEE Trans. Geosci. and Remote Sensing* 24(1): 90-98.

Xie, Y., Z. Sha, and M. Yu. 2008. Remote sensing imagery in vegetation mapping: A review. *J. Plant Ecology* 1(1): 9-23.

Zadoks, J. C., T. T. Chang, and C. F. Konzak. 1974. A decimal code for the growth stages of cereals. *Weed Research* 14(6): 415-421.